Nanostructured Titanosilicate Microspheres with Gallium and Lanthanum Based Nanocrystals

O. PONTA, S. SIMON

Babes-Bolyai University, Faculty of Physics & Institute for Interdisciplinary Research in Bio-Nano-Science 400084 Cluj-Napoca, Romania
E-mail: oponta@phys.ubbcluj.ro; simons@phys.ubbcluj.ro

Abstract. The aim of this study was to synthesize by sol-gel and spray drying amorphous titanosilicate microspheres gallium/lanthanum oxides, and to develop nanocrystalline phases by thermal treatments. Microspheres size was less than 5μm. The samples were slightly doped with Gd_2O_3 in order to receive EPR information on the surrounding of Gd^{3+} ions usually disposed in similar sites to that occupied by gallium or lanthanum. The changes induced in samples structure and morphology by Ga_2O_3 or La_2O_3 addition and by thermal treatments were investigated by XRD and SEM, FTIR, Raman and EPR spectroscopies. Beside anatase and rutile, Ga_2O_3 and $La_2Ti_2SiO_9$ nanocrystals were developed, all these crystalline phases being desired concerning their applications.

Key words: microspheres, titanosilicate, nanocrystals, sol-gel, spray drying.

1. Introduction

Silica-titania mixed oxides have ben of large interest [1-3], especially as catalysts and catalyst support materials, due to the fact that silica-titania nanocomposites have higher photoactivity than pure TiO_2. The presence of TiO_2–SiO_2 binary system compounds in photocatalytic field [4–6] is related to the advantages from both TiO_2, an n-type semiconductor with catalytic activity, and SiO_2, with high thermal stability and good mechanical strength, but some more by generation of new photoactive sites due to the interaction of TiO_2 and SiO_2 [7–9]. Not as extensive as in the field of photocatalysis, there is also a promising interest for titanosilicates in the field of biomaterials [10–14]. Nanosized titanium dioxide polymorphs (anatase and rutile) have wide applications ranging from a substance for white pigment to photocatalysts and nanoscale electronic devices, and they play also a role in the biocompatibility of bone implants. The performance of TiO_2 polymorphs in the mentioned applications strongly relies on their physicochemical

characteristics such as crystallinity, crystal size, specific area and surface characteristics [15]. Bulk and surface defects have an important role in many processes occurring at oxide surfaces, *e.g.* vacancies may serve as active sites facilitating adsorption of different species [16, 17].

The addition of rare earths (RE) may change the physical and chemical properties of titanosilicate systems. The doping with RE ions can change the particle morphology, and retard the crystalline grain growth during heat treatments [18], that is an important aspect in photocatalytic applications. The catalytic activity of TiO_2–SiO_2 generally increases with the addition of rare earth promoters [18]. The effect of rare earths addition on hydrophilicity of TiO_2/SiO_2 films was also reported, namely the hydrophilicity of pure TiO_2 film is enhanced by both SiO_2 and La_2O_3 [19]. In low concentration range of La_2O_3 this materials has applicability in both optical glass and biomaterials fields. It was reported that lanthanum enhances *in vitro* osteoblast differentiation but has no effect on type I collagen [20]. Interestingly, lanthanum is rapidly emerging as a major player in the management of multiple other systemic diseases especially in the field of oncology [21–23].

Taking into consideration the good catalytic activity of gallium sites [24] this study aims to investigate the SiO_2–Ti_2O system both with lanthanum oxide and with gallium oxide. The study is focussed on the effect of lanthanum and gallium as well as of the thermal treatment influence on the surface composition and structure of these titanosilicate systems because their physical and chemical surface properties are of major interest in different applications. A small amount of gadolinium was added, considering that the Gd^{3+} ($4f^7$,$^8S_{7/2}$) is a paramagnetic ion in the S state, frequently used as EPR sensors for structural investigations of noncrystalline and ceramic materials [25–27].

Specific thermal treatments were applied in order to develop controlled nanocrystals, oxygen vacancies and thermally stabilize the synthesized materials. It was chosen for the synthesis the sol-gel method combined with spray drying process because sol-gel method offers a good chemical homogeneity, low-temperature processing and allows the control of pore size distribution, while spray-drying is widely employed to solidify sols into fine powders, being a single-step process which can readily be scaled up [28]. Various complementary characterization techniques were used: *X-Ray Diffraction* (XRD), *Scanning and Electron Microscopy* (SEM), *Electron Paramagnetic Resonance* (EPR), *Fourier Transform Infrared* (FTIR) and Raman spectroscopies in order to obtain a clearer picture of the physico-chemical properties.

2. Experimental

Synthesis

$TiO_2 \cdot SiO_2$ microspheres with 5 mol % lanthanum or gallium oxide doped with gadolinium, hereinafter noted as 5Ga and 5La, have been prepared by a combined

sol-gel with spray drying methods. The spray dried microspheres were less than 5 μm in diameter. The sol was obtained by the hydrolysis and polycondensation of tetraethoxysilane-TEOS (98%, Aldrich) and titanium isopropoxide-TIP (98%, Merck) and is schematically presented in Fig. 1. Titanium isopropoxide $C_{12}H_{28}O_4Ti$ (TIP), tetraethoxysilane $Si(OC_2H_5)_4$ (TEOS), gadolinium nitrate $Gd(NO_3)_3{\cdot}6H_2O$, gallium nitrate $Ga(NO_3)_3{\cdot}6H_2O$, lanthanum nitrate $La(NO_3)_3{\cdot}6H_2O$ of p.a. purity were used as starting materials and 2-methoxiethanol as solvent (Table 1). The starting materials TEOS, TIP, gadolinium, gallium/lanthanum nitrates were mixed with 2-methoxyethanol in 1:2 mass ratio for the first two precursors, and 1:10 mass ratio for the last three, subsequently being stirred for 30 minutes in order to get a clear solution with high homogeneity. All these preparation steps were accomplished in air at room temperature. The solutions, in ratios accordingly to the desired composition, were mixed together for 15 minutes and the final solution was sprayed using a Buchi-290 Mini Spray-dryer device in order to obtain microspheres, according to the schematic representation given in Fig. 1. In spray drying, a solution or suspension is fed to an atomizer and the droplets formed are mixed with a hot gas. This causes the solvent of the droplets to evaporate, leaving a dry powder product. Using this technique the number of unit operations is reduced, improving production efficiency and reducing costs, especially since spray drying is a technique that can be easily automated and equipped for in-line product analysis.

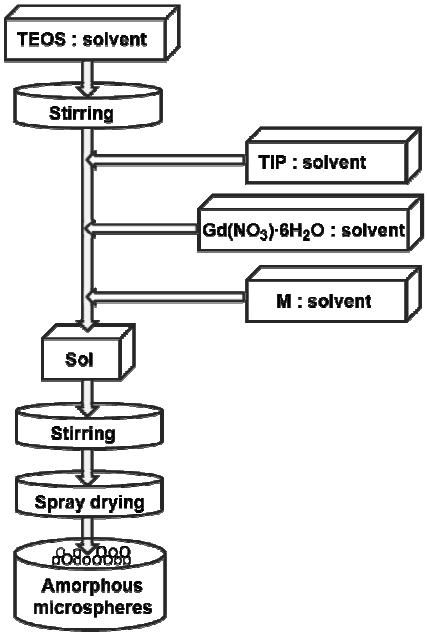

Fig. 1. Schematic representation of the samples synthesis (M = $Ga(NO_3)_3{\cdot}6H_2O$, $La(NO_3)_3{\cdot}6H_2O$).

Table 1. Precursors - solvent weight ratio

Starting materials		Ratio
Precursors	**Solvent**	**(weight %)**
TEOS	2-methoxyethanol	1:2
TIP		
$Gd(NO_3)_3 \cdot 6H_2O$		1:10
$Ga(NO_3)_3 \cdot xH_2O$		
$La(NO_3)_3 \cdot 6H_2O$		

For spray-drying we used an accessory Inert Loop B-295 and a 1.4 mm nozzle tip. The flow type was co-current with mixing of air and liquid at the nozzle head. The powder was collected using a cyclone. The air spray flow rate was 600 l/h and the aspirator rate was kept constant at 95%. The inlet temperature was controlled at 120°C. The outlet temperature (70°C) was determined by the inlet temperature and relative factors such as air and liquid flow rates. All processing parameters for the spray drying procedure were the same for both SiO_2–Ti_2O–La_2O_3 (5La) and SiO_2–Ti_2O–Ga_2O_3 (5Ga) samples. The resulted powders were white microsphere particles.

Three different thermal treatments, at 700, 900 and 1100°C, for 30 minutes, have been applied on samples in order to remove the remained precursors from synthesis process, to stabilize the sample and to develop the desired crystalline phases.

Experimental Techniques

The XRD patterns were recorded with a Shimadzu XRD–6000 diffractometer using Cu Ka (λ = 1.5405 Å) radiation, at a scan speed of 2º/min. Crystallographic identification was accomplished by comparing the experimental XRD patterns with those of JCPDS (Joint Committee on Powder Diffraction Standards: JCPDS#PDF) database for standard inorganic crystal structures. The average crystallite sizes were estimated based on Scherrer's formula [29]: $D = k\lambda/\beta \cos\theta$, where D is the average particle size, k is a constant equal to 0.89, λ is the wavelength of X-rays equal to 0.1542 nm (*i.e.* Cu Ka) and β is the full width at half maximum (FWHM) of the representative peak.

The morphology of the samples was explored by scanning electron microscopy (SEM) using a FEI QUANTA 3D FEG dual beam and Jeol JSM 5510LV scanning electron microscopes in high vacuum work mode. In order to amplify the secondary electrons signal a conductive Pt-Pd coating of 3 nm thickness was applied to the specimen into an Agar Automatic Sputter Coater, in Ar atmosphere.

FTIR spectroscopic analyses were realized with a JASCO 6200 FTIR spectrometer in the 4000 to 400 cm^{-1} range with a spectral resolution of 4 cm^{-1}. The

FTIR spectra were recorded from the mixture of the powder samples with KBr pressed into pellets. In order to compare the infrared absorption band intensities, we used the same sample amount (0.8 g) for all KBr pellets.

The Raman measurements were performed using a Raman Systems R3000 CN spectrometer equipped with a 785 nm diode laser coupled to a fiber optic probe. The spectra were recorded in one acquisition, 10 s integration time. The laser power on the sample was 150 mW.

Room temperature cw-EPR spectra were recorded in the magnetic field range of 700–4700 G, with ADANI 6400 EPR spectrometer, operating in X band (9.1–9.6 GHz). EPR glass capillaries of the same diameter were filled with samples of equal quantities. The spectrometer settings were: modulation frequency at 100 kHz, modulation amplitude at 1 G and power attenuation of 6 dB.

3. Results and Disccusion

X-Ray Diffraction Analysis

The X-ray diffraction patterns of the obtained samples presented in the Figs. 2 and 3, evidence the presence of nanocrystals in both systems. One can observe that lanthanum and gallium addition lead to different phase developments after 30 minutes heat treatments. After a calcination at 700°C, the sample with lanthanum (5La) remains amorphous (as revealed by the broad characteristic diffraction peak between 2θ ~ 20° and 30°, Fig. 3a), while the one with gallium develops anatase nanocrystals, identified by the diffraction lines at 2θ ~ 25.3° (101) and 2θ ~ 48.0° (200) (JCPD#PDF card No. 21-1272), of 4 nm in size. By increasing the thermal treatment up to 900°C beside the anatase nanocrystals the rutile phase have been observed in the 5 Ga sample (JCPD#PDF card No. 21-1276). In this sample the average crystallites size was found to be 5.5 and 9 nm for anatase and rutile, respectively (Table 1). If we take out the sample from the oven immediately after the temperature is reaching 900°C, only anatase phase is developed (see inset of the Fig. 2). After 30 minutes at 1100°C, the anatase phase disappeared and, beside rutile, nanocrystals of Ga_2O_3 have been developed.

Table 2. Mean crystallite size of the crystalline phases developed after heat treatment as derived from Scherrer formula

Samples	Heat treatment temperature (°C)	Phase	Cristallites size (nm)
5Ga	700	Anatase	4
	900	Anatase	5.5
		Rutile	9
	1100	Rutile	25
		Ga_2O_3	20
5La	700	amorphous	-
	900	Rutile	-
	1100	Rutile	27
		$La_2Ti_2SiO_9$	29

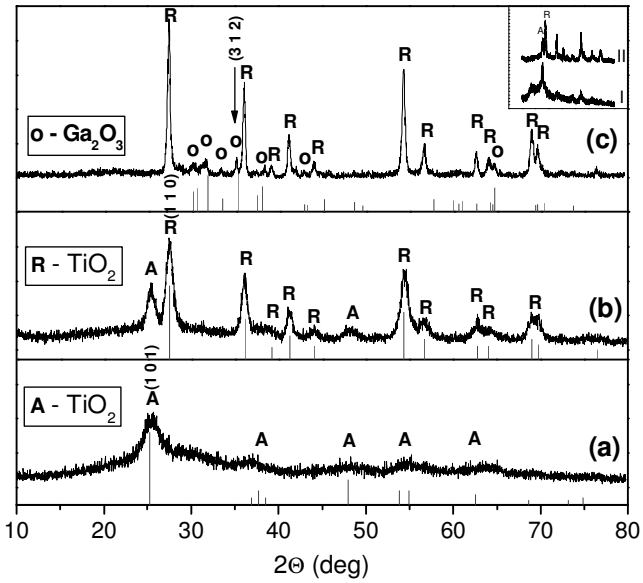

Fig. 2. The XRD patterns of 5Ga microspheres after 30 minutes calcination at 700 (a), 900 (b) and 1100°C (c). Inset: the XRD patterns of 5Ga microspheres (I) calcined at 900°C for 30 minutes, (II) removed from the oven once 900°C temperature was reached.

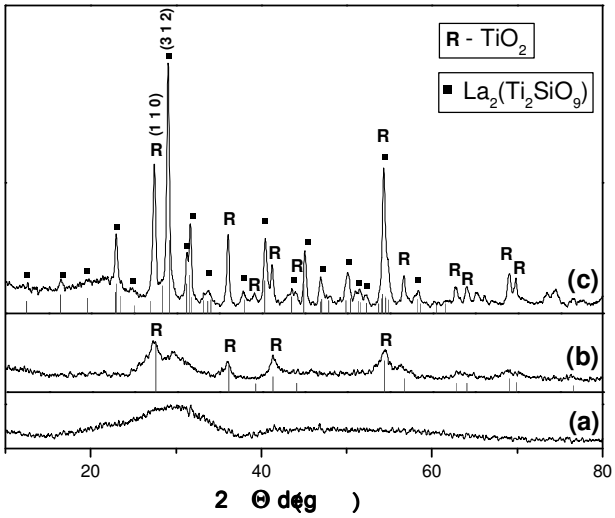

Fig. 3. The XRD patterns of 5La microspheres after 30 minutes calcination at 700 (a), 900 (b) and 1100 °C (c).

For the sample with lanthanum the transition from amorphous state is directly to the rutile phase, but only at 900°C, the nanocrystalites being too small for fair size

estimation. Moreover at this temperature, starts the $La_2Ti_2SiO_9$ (JCPD#PDF card No. 82-1490) nucleation process (Fig. 3). At a higher temperature both crystalline phases are now well developed, the crystals size being larger for the $La_2Ti_2SiO_9$ phase (Table 2).

Scanning Electron Microscopy

The SEM results show that the obtained particles after 30 minutes heat treatment at 700°C are well defined and have a spherical shape of less than 5 μm in diameter without visible pores on the surface (Figs. 4 and 5). In the case of gallium containing samples it can be observed, after all thermal treatments the presence of some nanocrystals on the surface. On the 700°C calcined 5Ga microspheres the formed nanocrystalites must be, accordantly with XRD pattern, of anatase type, while after 900°C thermal treatment the well evidenced crystals are of rutile type. The 1100°C heat treatment leads to an increase of the rutile nanocrystals, but also new nanocrystals, of different shape, appear. The crystals of acicular shape on these microspheres can be of Ga_2O_3 phase, according to XRD pattern of this sample.

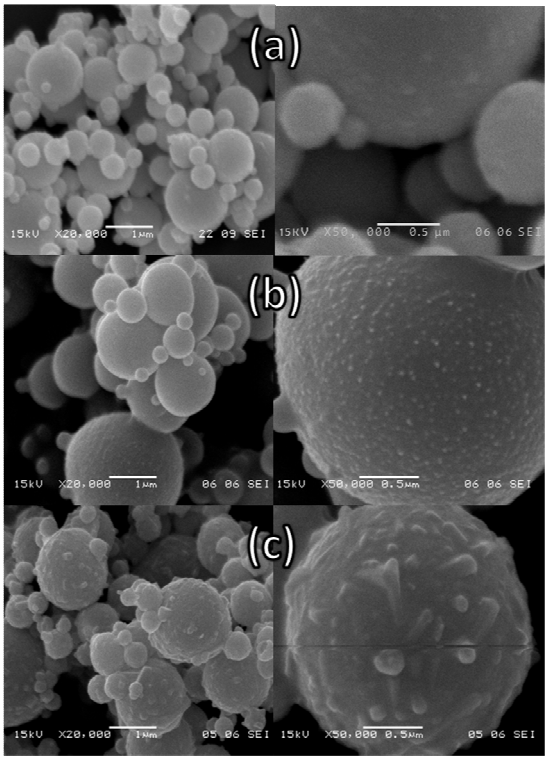

Fig. 4. SEM image of 5Ga samples at two different magnifications after 30 minutes heat treatment at 700 (a), 900 (b) and 1100°C (c).

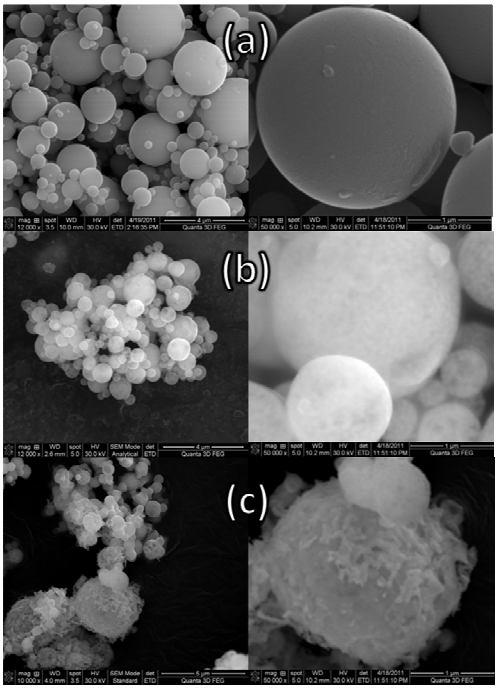

Fig. 5. SEM image of 5La sample at two different magnifications for 700 (a), 900 (b) and 1100°C (c) thermal treatment.

The SEM images for lanthanum containing samples are presented in the Fig. 5 for all three heat treatments. The 5La microspheres heat treated at 700°C that present an amorphous structure according to XRD pattern emphasized a smooth surface. At higher thermal treatments some changes occur on the 5La microspheres' surface, thereby it can be noticed a roughness of these microspheres surface compared with those annealed at 700°C. A different morphology can be observed at the highest calcination temperature (1100°C) (Fig. 5c). Related to XRD pattern (Fig. 3c) two types of nanocrystals, rutile and $La_2Ti_2SiO_9$ phase, are developing after 1100°C heat treatment temperature, the last one being the dominant one. The nanocrystals emphasized on the 5La microspheres surface can be related to $La_2Ti_2SiO_9$ phase, because the rutile crystals have different shape (Fig. 4.).

Fourier Transform Infrared Spectroscopy

The Figs. 6 and 7 present the FTIR spectra for the 5Ga and 5La microspheres, respectively. All these spectra are dominated by two broad absorption bands. First one is located in the intermediate region (1000-1300 cm^{-1}), while the second one in

the low wavenumber region (400–900 cm^{-1}). These broad bands are better resolved by increasing the thermal treatment due to the development of crystalline phases according to XRD patterns.

The broad absorption band located in the intermediate region has the maximum value in the 1000–1150 cm^{-1} spectral range and a shoulder (around 1200 cm^{-1}) whose contribution increases with the heat treatment applied. This band is assigned to asymmetric stretching mode of Si-O-Si group involving mainly oxygen motion along the Si–Si direction [30] (ASTO1 mode) of the tetrahedral SiO_4 co-ordination unit, while the shoulder can be ascribed to the longitudinal optical Si–O–Si stretching vibration (ASLO1 mode) [31-34]. The corresponding symmetric motion STO1 can be detected at 797 cm^{-1} [34–38] as a component of broad absorption band located in the low wavenumber region. In the 1000–1150 cm^{-1} wavenumber region is repered also the Ti-O-Si vibration [4, 37] around 1080 cm^{-1} that can overlay with the Si–O–Si vibration band above mentioned.

In the 900-1000 cm^{-1} spectral region can be observed a broad vibration band of low intensity. This band decrese in intensity for the sample with gallium content (5Ga), while for the 5La sample is better resolved (Figs. 6 and 7). The band can be assigned to the stretching of the $Si\text{-}O^-$ species of Si-O-Ti or $Si\text{-}O^-$ defects sites which are formed by the inclusion of Ti^{3+} ions into the SiO_2 matrices [38]. The existence of this absorption feature indicates that during the synthesis a process of linkages between the two networks, *i.e.* SiO_4 and TiO_6, occurs. The presence of oxygen vacancies is also evidenced in the EPR spectra presented in Figs. 10 and 11. Should be notice here that this broad band contains also the contribution of the silanol groups, (Si-OH) whose vibrations are usually present in FTIR spectra in this wavenumber region. For the sample with gallium content (5Ga) can be observed that the intensity of this band monotonically decreases by calcination. For this sample a segregation of silica take place by increaseing the thermal treatment and only Ga_2O_3 and TiO_2 cristaline phases are developed acording to XRD data (Fig. 2). Thus can be assume that the main contribution for this band are the silanol groups (Si-OH) stretching vibrations. In the FTIR spectra of the sample with lanthanum content (5La) the broad band is better resolved for the 1100°C calcination temperature (Fig. 7). For 5La sample beside TiO_2 nanocrystals, $La_2Ti_2SiO_9$ phase is developed with increasing the thermal treatment temperature, phase that involves both silicon and titanium (Fig. 3). Therefore, it can be concluded that this well resolved band around 955 cm^{-1} observed in the FTIR spectrum of the 1100°C thermal treated 5La sample is related to vibrations of Si-O-Ti bridges [34, 35, 39, 40].

In the low wavenumber region (400–900 cm^{-1}) of the sample with gallium content (5Ga) can be observed a band around 415 cm^{-1} for the microspheres thermal treated at 1100°C. For the 700°C calcined sample, this band is not present in the FTIR spectrum, but a week shoulder is visible at 900°C thermal treatment. This band is representative for rutile structure and the FTIR data are in good

agreement with the XRD results. The FTIR vibration band around 500 cm^{-1} are related to six-fold coordinated octahedral Ga [41]. This band increases in intensity by increasing the thermal treatment, being better resolved for 1100°C calcination temperature where the Ga_2O_3 nanocrystals are developed, according to XRD pattern (Fig. 2c). In the 570–800 cm^{-1} wavenumber region is present a broad absorption band with a shoulder around 830 cm^{-1}. This band is a convolution of the vibration mode of four-fold coordinated $[GaO4]^-$ structures (reported around 745 cm^{-1} [41]) and TiO_2 rutile vibrations (reported at 800–650 cm^{-1} [42, 43]), while the shoulder is related to Si-O in SiO_2 structure [44].

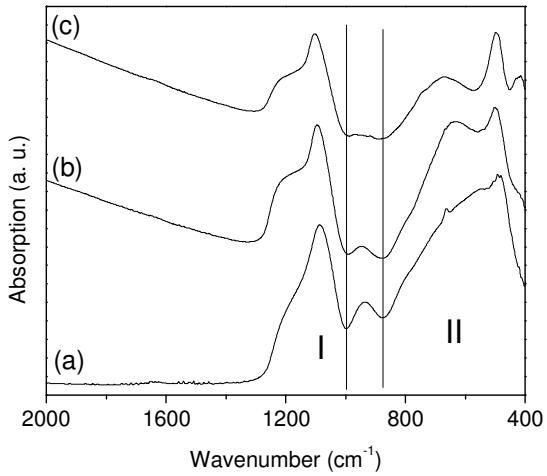

Fig. 6. FTIR spectra of the 5Ga sample thermal treated at 700 (a), 900 (b) and 1100°C (c).

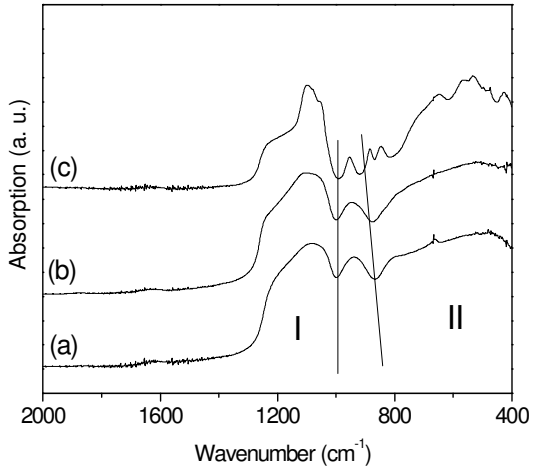

Fig. 7. FTIR spectra of the 5La sample thermal treated at 700 (a), 900 (b) and 1100°C (c).

The 5La FTIR spectra have characteristic shape of amorphous structures for the 700 and 900°C calcined microspheres. For the 1100°C thermal treatment the spectrum is better resolved due to the development of TiO_2 rutile and $La_2Ti_2SiO_9$ nanocrystals. The band located in the 1000–1300cm^{-1} spectral region is broader for the 5La microspheres compared with the 5Ga ones because it can contain also the contribution of La-O-Si vibration that is reported around 1065 cm^{-1} [45]. Moreover the La-O vibration can be evidenced in the low spectral region around 515 and 475 cm^{-1} [46, 47].

In the FTIR spectra of the both 5Ga and 5La samples (Figs. 6 and 7), the vibration bands at around 1640 cm^{-1} are associated with the presence of molecular water. By increasing the heat treatment temperature, this band become weaker suggesting the gradual evaporation of OH groups [48].

Raman Spectroscopy

In the Figs. 8 and 9 are presented the Raman spectra of the microspheres with gallium (5Ga) and lanthanum (5La) content, respectively. Only the microspheres thermal treated at 1100°C for the both gallium and lanthanum containing samples and the ones calcined at 900°C for 5La evidenced Raman bands, for the rest the fluorescence phenomena covered the Raman signal. The Fig. 8 presents the Raman spectrum of the 5Ga microspheres thermal treated at 1100°C in comparison with the Raman spectrum of pure TiO_2 rutile (RRUFF ID: R050031) and can be observed three vibration bands around 235, 445 and 610 cm^{-1} and a shoulder at 700 cm^{-1}. All these Raman vibration bands are related to TiO_2 rutile nanocrystals, the results being in agreement with XRD results where the rutile diffraction lines dominate the pattern.

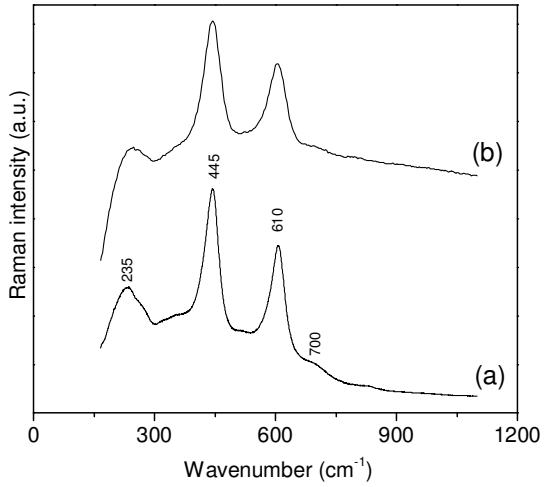

Fig. 8. Raman spectra of the (a) 1100°C heat treated 5Ga microspheres and (b) pure TiO_2 rutile (RRUFF ID: R050031).

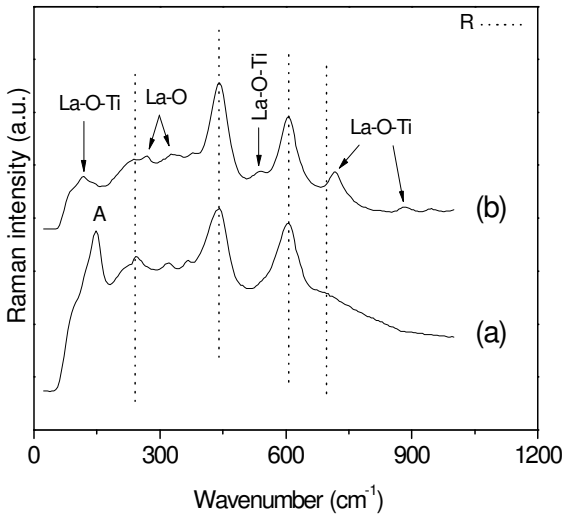

Fig. 9. Raman spectra of the (a) 900 and (b) 1100°C heat treated 5La microspheres.

The characteristic Raman bands of TiO_2 rutile are also evidenced in the Raman spectra of the microspheres with lanthanum content for both thermal treatments presented in Fig. 9. Beside the specific bands for rutile there is visible some other features around: 120, 150, 270, 335, 530, 710 and 885 cm^{-1}. The Raman bands around 270 and 335 cm^{-1} are related with La-O vibration [49], while the 120, 530, 710 and 885 cm^{-1} are characteristic to La-O-Ti vibrations [50].

Moreover the 900°C calcined microspheres (5La) present in the low wavenumber region a Raman band around 150 cm^{-1}, which is the characteristic peak of anatase crystallise phase. In the XRD pattern (Fig. 3b) cannot be evidenced the anatase diffraction lines, thus can be concluded that the crystallite size for anatase phase is under XRD resolution.

Electron Paramagnetic Resonance Spectroscopy

The gadollinium doping is allowing to obtain aditional information about the structure and local order. The Gd^{3+} ions are paramagnetic resonance centres sensitive to their surrounding that can give details about the structural changes occurred in their vicinity[51–55]. These changes can occurred due the different composition of the microspheres (adition of gallium or lanthanum oxide) and the crystallinity degree induced by the thermal treatments. The Figs. 10 and 11 are presented the EPR spectra of the microspheres with gallium and lanthanum content, respectively at 700, 900 and 1100°C temperature. For the microspheres heat treated up to 900°C is evidenced in the both systems three EPR signals at g ~ 5.9, 2.8 and 2.0. These are typical signals of Gd^{3+} ions located at sites with

intermediate and weak crystal fields respectively, a characteristic of so called U-spectrum of Gd^{3+} ions in disordered matrices. This is the most frequent signature of S-state rare earth ions in such materials [52, 55–57].

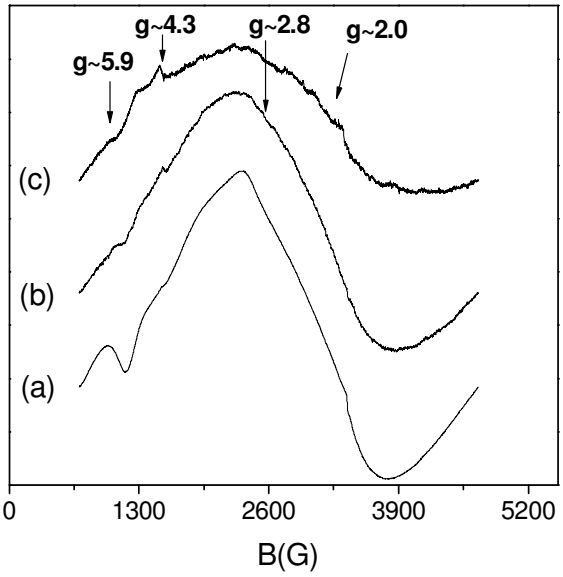

Fig. 10. EPR spectra of the 5Ga microspheres thermal treated at 700 (a), 900 (b) and 1100°C (c).

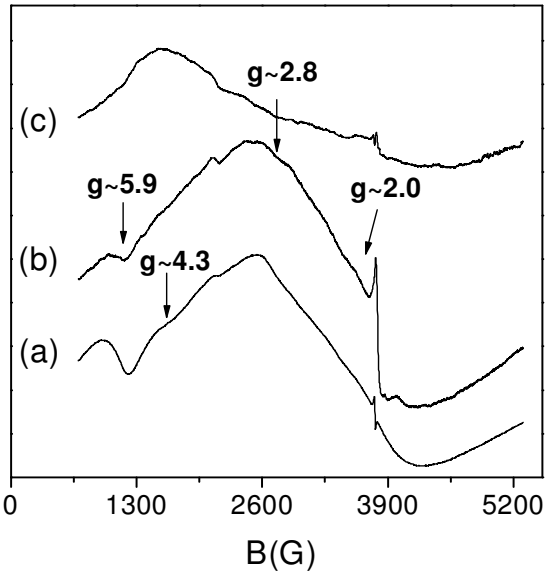

Fig. 11. EPR spectra of the 5La microspheres thermal treated at 700 (a), 900 (b) and 1100°C (c).

The structural changes induced by the calcination are well reflected in the EPR spectra of the both systems (Figs. 10 and 11). One can observed that the large EPR line at g ~ 2.0 dominates the spectra. This signal directly reflects the changes in the spin-lattice relaxation rate and most importantly the structural disoder around Gd^{3+} ions. Except the 1100°C annealed sample with lanthanum can be assume that Gd^{3+} ions are preponderantely disposed in the residual non-crystalline phase, experiencing weak crystal fields, resulting from structural relaxation, but with still a high degree of disorder around them [52–55]. Moreover the small features at g ~ 5.9 and 2.8 indicates that there are sites in the non-crystalline matrices where the Gd^{3+} ions are experiencing intermediate field. The EPR spectrum of the 1100°C thermal treated sample with lanthanum is assigned to Gd^{3+} ions distributed in lantanum site from the $La_2Ti_2SiO_9$ developed phase. The line at g ~ 4.3 is assigned to iron (III) that appears because of iron impurities.

All the spectra have an sharp signal overlapped on the large EPR line at g ~ 2.0 that dominates the spectra. This signal is more pronounced in the microspheres with lanthanum and can be attributed to oxygen vacancies, a bulk defect, probably an electron trapped on an oxygen vacancy. Can be observed in the EPR spectra that the samples with lanthanum content have larger amount of oxygen vacancies compared with the gallium content samples.

4. Conclusions

SiO_2-Ti_2O-M_2O_3 (M = Ga, La) microspheres of less than 5 μm in diameter with active surface were synthesized by sol-gel process combined with spray drying method titanosilicate. Activation was realized by nanocrystals development on surface after heat treatments.

TiO_2 rutile phase was induced by 1100°C heat treatment as confirmed by XRD and FTIR and Raman spectroscopies. Beside rutile, $La_2Ti_2SiO_9$ phase was developed in the lanthanum containing sample, and Ga_2O_3 in the sample with gallium. Anatase phase was evidenced by X-ray diffraction in lanthanum containing sample up to 900°C, but not in gallium containing sample, even Raman analysis highlighted a band characteristic for anatase, and suggests that the crystallites size is under the XRD detection limit. The developed nanocrystals were clearly shown by SEM analysis. While the gallium is posponing the transition temperature of anatase to rutile, so that microspheres can be of interes for catalitical reactions, supported by anatase, at quite high temperatures (up to 900°C), the lantanum it not favorable for anatase phase formation, but is posponing the microsperes crystalization. After heat treatment at higher temperature (1100°C), both samples are presenting on their surface rutile nanocrystals but toghether with galium oxide nanocrystals or of $La_2Ti_2SiO_9$ phase. These microspheres taped with such mixtures of nanocrystals are candidates for different applications in the fields like catalysis and biomedical applications.

References

[1] A.A. ISMAIL, I.A. IBRAHIM, M.S. AHMED, R.M. MOHAMED, H. ELL-SHALL, J. Photochem. Photobiol. **A163**, pp. 445, 2004.

[2] M.S. VOHRA, K. TANAKA, Wat. Res. **37**, pp. 3992, 2003.

[3] Z. FENG, L. KAIMING, W. GUOLIANG, S. HUA, H. ANMIN, J. Cryst. Growth **264**, pp. 297, 2004.

[4] Y. ZANG, Y. WU, M. CHEN, L. WU, Colloid Surface **A353**, 216, 2010.

[5] W. DONG, C.W. LEE, X. LU, Y. SUN, W. HUA, G. ZHUANG, S. ZHANG, J. CHEN, H. HOU, D. ZHAO, Appl. Catal. **B95**, pp. 197, 2010

[6] X. GAO, I.E. WACHS, Catal. Today **51**, pp. 233, 1999.

[7] T.V. NGUYEN, O.B. YANG, Catal. Today **87**, pp. 69, 2003.

[8] F. MEI, C. LIU, L. ZHANG, F. REN, L. ZHOU, W.K. ZHAO, Y.L. FANG, J. Cryst. Growth. **292**, pp. 87, 2006.

[9] V. PÂRVULESCU, V.I. PARVULESCU, G. POPESCU, A. JULBE, C. GUIZARD, L. COT, Catal. Today **25**, pp. 385, 1995.

[10] M.S. DADASH, S. KARBASI, M.N. ESFAHANI, M.R. EBRAHIMI, H. VALI, J. Mater. Sci. Mater. Med. **22**, pp. 829, 2011.

[11] S. AREVA, V. AARITALO, S. TUUSA, M. JOKINEN, M. LINDEN, T. PELTOLA, J. Mater. Sci. Mater. Med. **18**, pp. 1633, 2007.

[12] A. CHENITI, O. PONTA, L. TIRLE, T. RADU, S. SIMON, J. Optoelectron. Adv. Mat. **6**, pp. 560, 2012.

[13] O. PONTA, E. VANEA, A. CHENITI, P. BERCE, S. SIMON, Mater. Chem. Phys. **135**, pp. 863, 2012.

[14] O. PONTA, C. GRUIAN, E. VANEA, B. OPREA, H.-J. STEINHOFF, S. SIMON, J. Mol. Struct. **1044**, pp. 2, 2013.

[15] J. MATTHIESEN, *The influence of point defects on TiO_2(110) surface properties*, A scanning tunneling microscopy study: PhD thesis, Editor: Interdisciplinary Nanoscience Center (iNANO), 2007.

[16] U. DIEBOLD, Surf. Sci. Rep. **48**, pp. 53, 2003.

[17] M.V. GANDUGLIA-PIROVANO, M. HOFFMAN, J. SAUER, Surf. Sci. Rep. **62**, pp. 219, 2007.

[18] R.M. MOHAMED, I.A.MKHALID, J. Alloy. Compd. **501**, pp. 143, 2010.

[19] K. GUAN, Y. YIN, Mater. Chem. Phys. **92**, pp. 10, 2005.

[20] X. WANG, L. YUAN, J. HUANG, T.-L. ZHANG, K. WANG, J. Cell. Biochem. **105**, pp. 1307, 2008.

[21] S. KAPOOR, J. Cell. Biochem. **106**, pp. 193, 2009.

[22] L. Feng, H. Xiao, X. He, Z. Li, F. Li, N. Liu, Z. Chai, Y. Zhao, Z. Zhang, Neurotoxicol. Teratol. **28**, pp. 119, 2006.

[23] G. FEI, L. YUANLEI, W. YANG, X. AN, L. GUOHUI, J. Rare Earths **25**, pp. 359, 2007.

[24] J.R. MOWRY, R.F. ANDERSON, J.A. JONSON, J. Oil Gas **83**, pp. 128, 1985.

[25] D.L. GRISCOM, J. Non-Cryst. Solids **67**, pp. 81, 1984.

[26] L.E. ITON, C.M. BRODBECK, S.L. SUIB, G.D. STUCKY, J. Chem. Phys. **79**, pp. 1185, 1983.

[27] C. LEGEIN, J.Y. BUZARE, G. SILLY, C. JACOBONI, J. Phys.: Cond. Matter **8**, pp. 4339, 1996.

[28] P. KORTESUO, M. AHOLA, M. KANGAS, I. KANGASNIEMI, A. YLI-URPO, J. KIESVAARA, Int. J. Pharm. **200**, pp. 223, 2000.

[29] J.I. LANGFORD, A.J.C. WILSON, J. Appl. Cryst. **11**, pp. 102, 1978.

[30] A.G. KALAMPOUNIAS, Bull. Mater. Sci. **34**, pp. 299, 2011.

[31] A. VULPOI, L. BAIA, S. SIMON, V. SIMON, Mater Sci Eng. **C32**, pp. 178, 2012.

[32] A. CHRISSANTHOPOULOS, N. BOUROPOULOS, S.N. YANNOPOULOS, Vib. Spectrosc. **48**, pp. 118, 2008.
[33] O. PONTA, R. CICEO-LUCACEL, A. VULPOI, T. RADU, S. SIMON, J. Biomed. Mater. Res. A DOI:10.1002/jbma.34989.
[34] R.F.S. LENZA, W. L. VASCONCELOS, Mater. Res. **5**(4), pp. 497, 2002.
[35] M. SCHRAML-MARTH, K.L. WALTHER, A. WOKAN, B.E. HANDY, A. BAIKER, J. Non. Cryst. Solids **143**, pp. 93, 1992.
[36] W.T. MINEHAN, G.L. MESSING, C.G. PANTANO, J. Non. Cryst. Solids **108**, pp. 163, 1989.
[37] V. ZELENAK, V. HORNEBECQ, S. MORNET, O. SCHAEF, P. LLEWELLYN, Chem. Mater. **1814**, pp. 3184, 2006.
[38] Y. KOTANI, A. MATSUDA, M. TATSUMISAGO, T. MINAMI, J. Sol-Eel Sci. Technol. **19,** pp. 585. 2000.
[39] S. KLEIN, S. THORIMBERT, W.F. MAIER, J. Catal. **163**, pp. 476, 1996.
[40] P. YAO, W. HU, Y. BAO, C. ZHANG, B. ZHU, W. LIU, Y. BAI, J. Ceram. Process. Res. **12**(3) 289, 2011.
[41] L.G. HWA, Y.R. CHANG, W.C. CHAO, Mater Chem Phys **85**, pp. 158, 2004.
[42] W. HAITAO, S. MENG, P. XU, W. ZHONG, Q. DU, Published online in Wiley DOI: 10.1002/pen.20708.
[43] A. PIRSON, A. MOHSINE, P. MARCHOT, B. MICHAUX, O.V. CANTFORT, J.P. PIRARD, A.J. LECLOUX, J. Sol-Gel Sci. Technol. **4**, pp. 179, 1995.
[44] G. TZVETKOV, N. MINKOVA, J. Mater. Sci. **35**, pp. 2435, 2000.
[45] S. CELERIER, C. LBERTY, F ASART, P. LENORMAND, P. STEVENS, Ceram. Int. **32**, pp. 271, 2006.
[46] E. RODRIGUEZ-REYNA, A.F. FYENTS, M. MCZKA, J. HANUZA, K. BOULAHYA, U. AMADOR, J. Solid State Chem. **197**, pp. 522, 2006.
[47] Y. IMANAKA, T. MASUI, Y. KATO, J. Solid State Chem. **178**, pp. 395, 2005.
[48] A. JENTYS, G. WARECKA, M. DEREWINSKI, J.A. LERCHER, J. Phys. Chem. **93**, pp. 4837, 1989.
[49] Z.L. ZHANG, C.T. AU, K.R. TSAI, Appl. Catal. **62**, pp. L29, 1990.
[50] K. KRISHNANKUTTY, K.R. DAYAS, Bull. Mater. Sci. **31**(6), pp. 907, 2008.
[51] D.L. GRISCOM, J. Non. Cryst. Solids **40**(211), pp. 272, 1980.
[52] S. SIMION, A.D. UDVAR, J. Am. Ceram. Soc. **93**, pp. 2760, 2010.
[53] S. SIMON, R. POP, V. SIMON, M. COLDEA, J. Non-Cryst. Solids **331**, pp. 1, 2003.
[54] E. CULEA, L. POP, S. SIMON, Mater. Sci. Eng. **B112**, pp. 59, 2004.
[55] O. PONTA, H. MOCUTA, M. VASILESCU, S. SIMON, J Sol-Gel Sci Technol, **58**(2), pp. 530, 2011.
[56] N.S. HUSSAIN, Y. PRABHAKARA REDDY, S. BUDDHUDU, Mater. Res. Bull. **36**, pp. 1813, 2001.
[57] J. KLIAVA, A. MALAKHOVSKII, I. EDELMAN, A. POTSELUYKO, E.A. PETRAKOVSKAJA, S. MELNIKOVA, T. ZARUBINA, G. PETROVSKII, Y. BRUCKENTAL, Y. YESHURUN, Phys. Rev. **B71**, pp. 104406, 2005.